



Genetics and Molecular Biology | Full-Length Text

## Biochemical characterization of Mycobacterial RNA polymerases

Stephanie L. Cooper,<sup>1</sup> Ryan M. Requijo,<sup>2</sup> Aaron L. Lucius,<sup>2</sup> David A. Schneider<sup>1</sup>

**AUTHOR AFFILIATIONS** See affiliation list on p. 18.

ABSTRACT Tuberculosis is caused by the bacterium *Mycobacterium tuberculosis* (Mtb). While eukaryotic species employ several specialized RNA polymerases (Pols) to fulfill the RNA synthesis requirements of the cell, bacterial species use a single RNA polymerase (RNAP). To contribute to the foundational understanding of how Mtb and the related non-pathogenic mycobacterial species, *Mycobacterium smegmatis* (Msm), perform the essential function of RNA synthesis, we performed a series of *in vitro* transcription experiments to define the unique enzymatic properties of Mtb and Msm RNAPs. In this study, we characterize the mechanism of nucleotide addition used by these bacterial RNAPs with comparisons to previously characterized eukaryotic Pols I, II, and III. We show that Mtb RNAP and Msm RNAP demonstrate similar enzymatic properties and nucleotide addition kinetics to each other but diverge significantly from eukaryotic Pols. We also show that Mtb RNAP and Msm RNAP uniquely bind a nucleotide analog with significantly higher affinity than canonical nucleotides, in contrast to eukaryotic RNA polymerase II. This affinity for analogs may reveal a vulnerability for selective inhibition of the pathogenic bacterial enzyme.

**IMPORTANCE** Tuberculosis, caused by the bacterium *Mycobacterium tuberculosis* (Mtb), remains a severe global health threat. The World Health Organization (WHO) has reported that tuberculosis is second only to COVID-19 as the most lethal infection worldwide, with more annual deaths than HIV and AIDS (WHO.int). The first-line treatment for tuberculosis, Rifampin (or Rifampicin), specifically targets the Mtb RNA polymerase. This drug has been used for decades, leading to increased numbers of multi-drug-resistant infections (Stephanie, *et al*). To effectively treat tuberculosis, there is an urgent need for new therapeutics that selectively target vulnerabilities of the bacteria and not the host. Characterization of the differences between Mtb enzymes and host enzymes is critical to inform these ongoing drug design efforts.

**KEYWORDS** *Mycobacterium tuberculosis*, tuberculosis, RNAP, enzyme kinetics, RNA synthesis, transcription, elongation complex

Synthesis of RNA from a DNA template, known as transcription, is an essential process in all organisms and a key point for the regulation of gene expression (1). In eukaryotic cells, RNA synthesis is catalyzed by at least three, nuclear, DNA-dependent RNA polymerases known as Pols, e.g., Pol I, Pol II, and Pol III (2). In bacteria, all RNA synthesis is performed by a single RNA polymerase (RNAP) (2). While the function of these enzymes is conserved across the domains of life, there is a significant divergence of structure and enzymatic properties. By characterizing the properties unique to bacterial RNAPs in comparison to eukaryotic Pols, we will not only identify the mechanisms by which bacteria accomplish gene expression but also reveal new potential vulnerabilities that could be exploited for therapeutic gain.

Much of our understanding of transcription in bacteria comes from studies of *Escherichia coli* (*E. coli*) as a model organism (1–6). The claw-like, five subunit core RNAP enzyme, composed of  $\beta$ ,  $\beta'$ ,  $\omega$ , and two identical copies of  $\alpha$ , is conserved

**Editor** Patricia A. Champion, University of Notre Dame, Notre Dame, Indiana, USA

Address correspondence to David A. Schneider, dschneid@uab.edu, or Aaron L. Lucius, allucius@uab.edu.

The authors declare no conflict of interest.

See the funding table on p. 18.

Received 18 June 2024 Accepted 28 August 2024 Published 24 September 2024

Copyright © 2024 American Society for Microbiology. All Rights Reserved.

October 2024 Volume 206 Issue 10

across the domain Bacteria (7). However, the amino acid sequences of these subunits are not identical across bacterial species (7). Members of the phylum Actinobacteria, such as Mycobacterium tuberculosis (Mtb) and the non-pathogenic strain, Mycobacterium smegmatis (Msm), have a lineage-specific insertion in the  $\beta'$  subunit that is absent in E. coli RNAP (8). The effect of this insertion and its potential evolutionary advantage have not yet been defined. Additionally, insertions such as SI3 in E. coli RNAP, characterized in polymerase pausing, are not present in *Mycobacterial* RNAPs (9).

It is becoming clear that Mycobacterial species, such as Mtb and Msm, are significantly different from E. coli not only with regard to the RNAP but also in terms of transcription factors, transcription initiation kinetics, and transcription termination (7-14). For example, the transcription factor NusG has been shown to induce pausing by Mtb RNAP but is an anti-pausing factor for E. coli RNAP (13, 15). Although extensive work has been done regarding transcription initiation, little is known about the elongation phase of transcription in Mycobacterial species (7). In this study, we present transient-state kinetic analyses of nucleotide addition catalyzed by Mtb RNAP and Msm RNAP. We characterize the mechanism of nucleotide addition shared by the enzymes and reveal how this mechanism is distinct from the mechanisms deployed by eukaryotic Pols I, II, and III (15-19). We also identify a sensitivity of Mtb RNAP for binding nucleotide analogs, a feature that could potentially be exploited for therapeutic benefit.

#### **RESULTS**

## Single nucleotide addition catalyzed by Mtb RNAP and model-independent kinetic analysis

Using our established promoter-independent in vitro transcription experimental design, we measured single nucleotide addition catalyzed by Mtb RNAP over a range of [ATP]. In this experiment, the RNAP is pre-bound to an RNA:DNA hybrid comprised of a 9-nucleotide (9-mer) RNA primer annealed to a complementary template DNA strand of a total length of 64 nucleotides. Following the addition of the RNAP to the RNA:DNA hybrid, the sample is incubated for sufficient time to allow for binding equilibrium, then the fully complementary non-template DNA strand is added to form an active elongation complex (EC; Fig. 1A). The polymerase radiolabels the RNA by the addition of  $\alpha^{-32}$ P-CTP as the next cognate nucleotide, resulting in visualizable RNA products (Fig. 1A). The labeled ECs are loaded into one syringe of a chemical quench flow, see Materials and methods. In the opposite syringe are a solution of ATP, magnesium, and heparin. Heparin ensures single turnover conditions by serving as a trap for unbound RNAPs (Fig. 1B) (18-25).

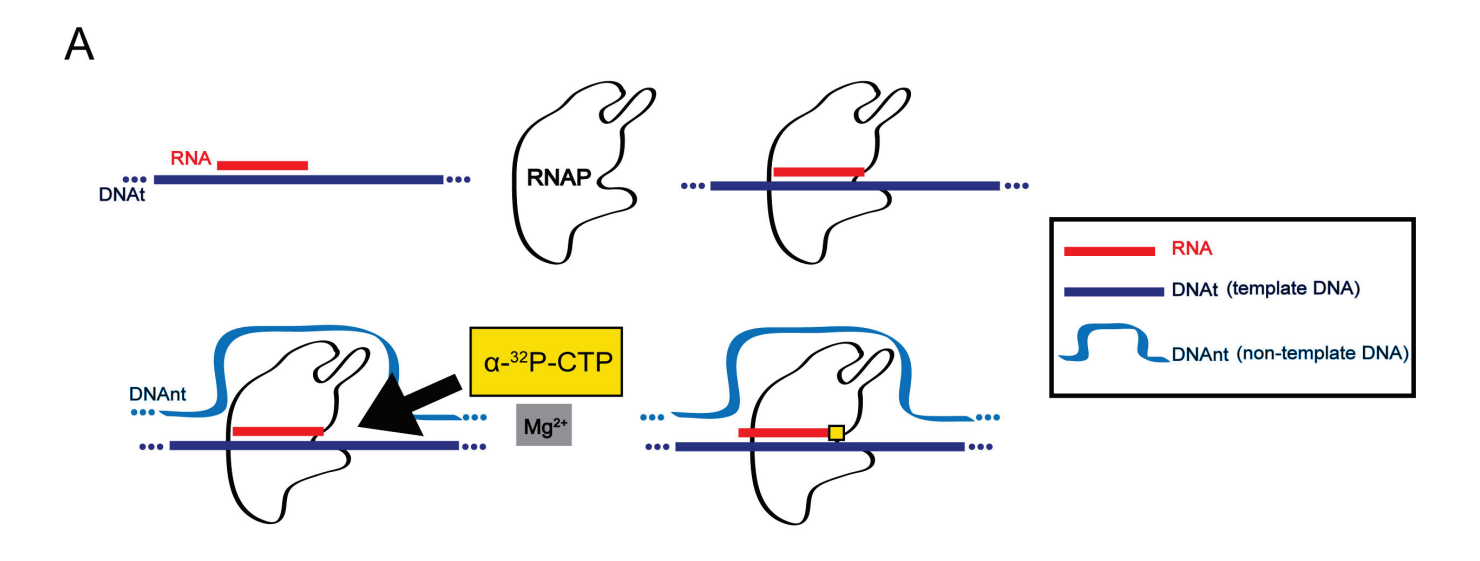
Using the quench flow, time courses of nucleotide addition are collected over reactions times of 5 ms to 10 s (Fig. 1B). Discrete reactions are collected by rapidly mixing the contents of the two syringes, followed by quenching of the reaction by rapidly mixing with 1 M HCl (Fig. 1B). Over the user-defined reaction time, the RNAP adds a single ATP as the next cognate nucleotide, forming the 11-mer RNA species (Fig. 1C). The proportion of 11-mer RNA is quantified via pixel density of the radiolabeled signal and normalized to the intensity of the starting material (18).

Following quantification of the formation of the 11-mer, time courses are plotted, and the time points are subjected to nonlinear least squares (NLLS) using a single or sum of two exponentials (Fig. 2A). We observed that at low [ATP], the time courses were well described by the sum of two exponentials (equation 1), whereas at [ATP] ≥250 µM, the time courses were well described by a single exponential (equation 2).

RNA fraction 
$$= A_{k_{\text{high}}} \left( 1 - e^{-(k_{\text{high}})t} \right) + A_{k_{\text{low}}} \left( 1 - e^{-(k_{\text{low}})^t} \right)$$
 (1)  
RNA fraction  $= A \left( 1 - e^{-(k_{\text{obs}})^t} \right)$  (2)

RNA fraction = 
$$A(1 - e^{-(k_{\text{obs}})^t})$$
 (2)

The simplest explanation for this observation is that nucleotide addition by Mtb RNAP requires two partially rate-limiting steps, one of which is undetectably fast at elevated [ATP] (Fig. 2A). We observed the same [ATP] threshold in the parallel experiments with



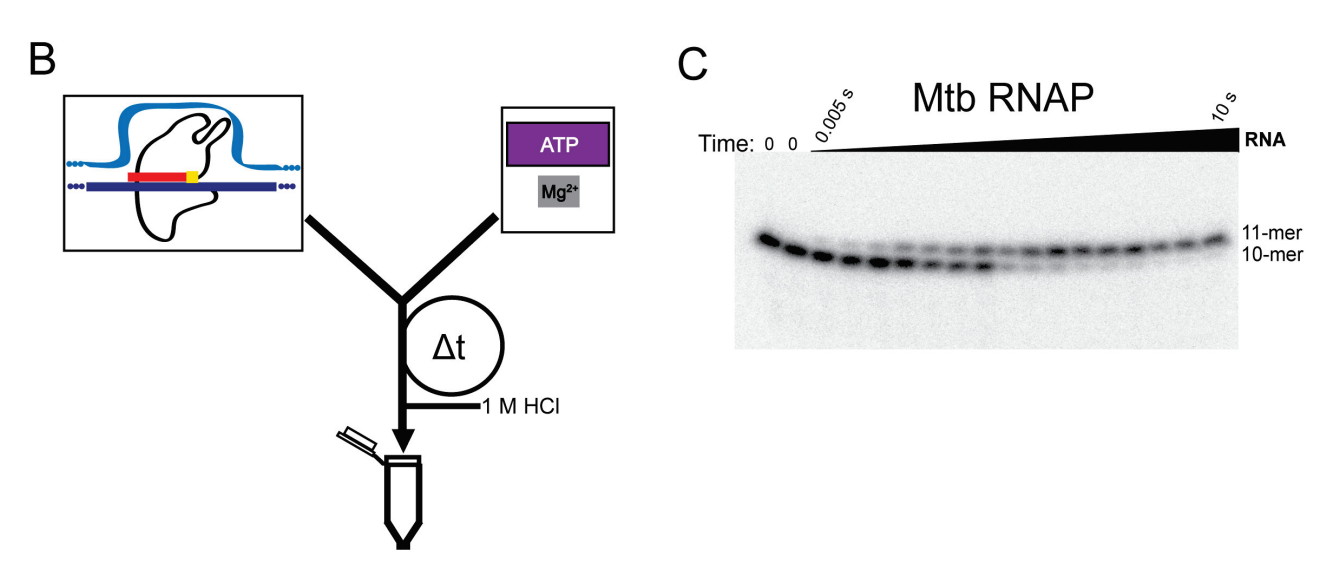


FIG 1 Capture of single nucleotide addition catalyzed by Mtb RNAP or Msm RNAP on the ms time scale. (A) Schematized promoter-independent EC formation and radiolabeling. (B) Schematized chemical quench flow rapid-mixing technique. (C) Representative gel image of RNA synthesis catalyzed by Mtb RNAP. The first two lanes are time zeros, representing only the starting radiolabeled 10-mer RNA.

Msm RNAP (Fig. 2B). We hypothesize that these results reveal two populations of ECs: one population of complexes that is elongation competent and another population of complexes that must undergo a transition to become elongation competent (discussed further below).

We then plotted the observed rate-constant vs [ATP] from the analysis for Mtb RNAP and Msm RNAP (Fig. 2C and D; Tables S1.1 and S1.2). From these plots, we identified the maximal observed rate constant,  $k_{\text{obs,max}}$ , and the binding affinity parameter  $K_{1/2}$ . Mtb RNAP  $k_{\text{obs,max}}$  for ATP =  $(14.4 \pm 1.9)$  s<sup>-1</sup>, and  $K_{1/2}$  for ATP =  $(162 \pm 73)$   $\mu$ M. For Msm RNAP, the  $k_{\text{obs,max}}$  for ATP =  $(20 \pm 1.6)$  s<sup>-1</sup>, and  $K_{1/2}$  for ATP =  $(243 \pm 58)$   $\mu$ M (Fig. 2C and D; Tables S1.1 and S1.2). These values are not within error for both RNAPs but are of similar magnitude, suggesting shared maximal rate constants of ATP addition and similar ATP-binding affinity.

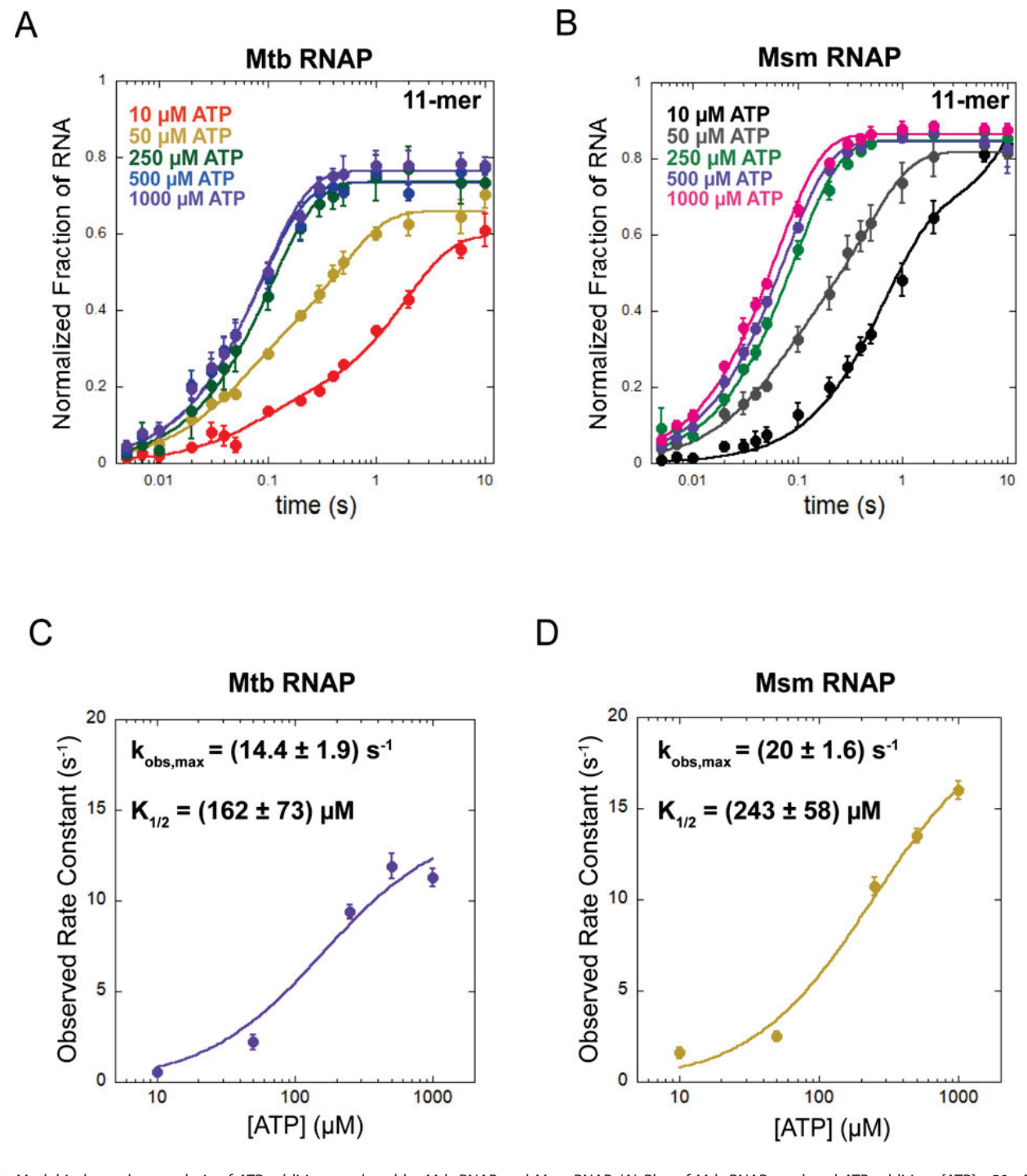


FIG 2 Model-independent analysis of ATP addition catalyzed by Mtb RNAP and Msm RNAP. (A) Plot of Mtb RNAP-catalyzed ATP addition. [ATP]  $\leq$ 50  $\mu$ M ATP are fit to equation 1, and [ATP]  $\geq$ 250  $\mu$ M ATP are fit to equation 2. (B) Plot of Msm RNAP-catalyzed ATP addition. [ATP]  $\leq$ 50  $\mu$ M ATP are fit to equation 1, and [ATP]  $\geq$ 250  $\mu$ M ATP are fit to Eq. 2. (C) Secondary plot of Mtb RNAP ATP addition, with calculated parameters. (D) Secondary plot of Msm RNAP ATP addition, with calculated parameters. Data points represent the average of three experimental replicates, and error bars represent the SD.

## Model-independent analysis of Sp-ATP- $\alpha$ -S incorporation catalyzed by Mtb RNAP

To further probe the rate-limiting step of nucleotide addition catalyzed by Mtb RNAP, we employed a slowly hydrolyzable analog of ATP, Sp-ATP- $\alpha$ -S. This nucleotide analog is used in biochemical applications to perturb the bond formation step and identify changes in nucleotide binding affinity (21). Time courses of Sp-ATP- $\alpha$ -S addition were collected

by assembling active ECs as previously described, as well as radiolabeling the RNA products with  $\alpha$ - $^{32}$ P-CTP (Fig. 1A). The chemical quench flow was not needed because we found that the incorporation of Sp-ATP-a-S is substantially slower than ATP. Instead, active, radiolabeled ECs formed with Mtb RNAP were mixed by hand with a solution of Sp-ATP- $\alpha$ -S, magnesium, and heparin. Resultant time courses were then subjected to NLLS using equation 2 (Fig. 3A). We performed the parallel study of Sp-ATP- $\alpha$ -S addition catalyzed by Msm RNAP (Fig. 3B).

To determine the impact of Sp-ATP- $\alpha$ -S on the kinetics of bond formation catalyzed by Mtb RNAP and changes in binding affinity, plots of the maximal observed rate constant ( $k_{\text{obs.max}}$ ) vs [Sp-ATP- $\alpha$ -S] were constructed (Fig. 3C; Table S2.2). We observe

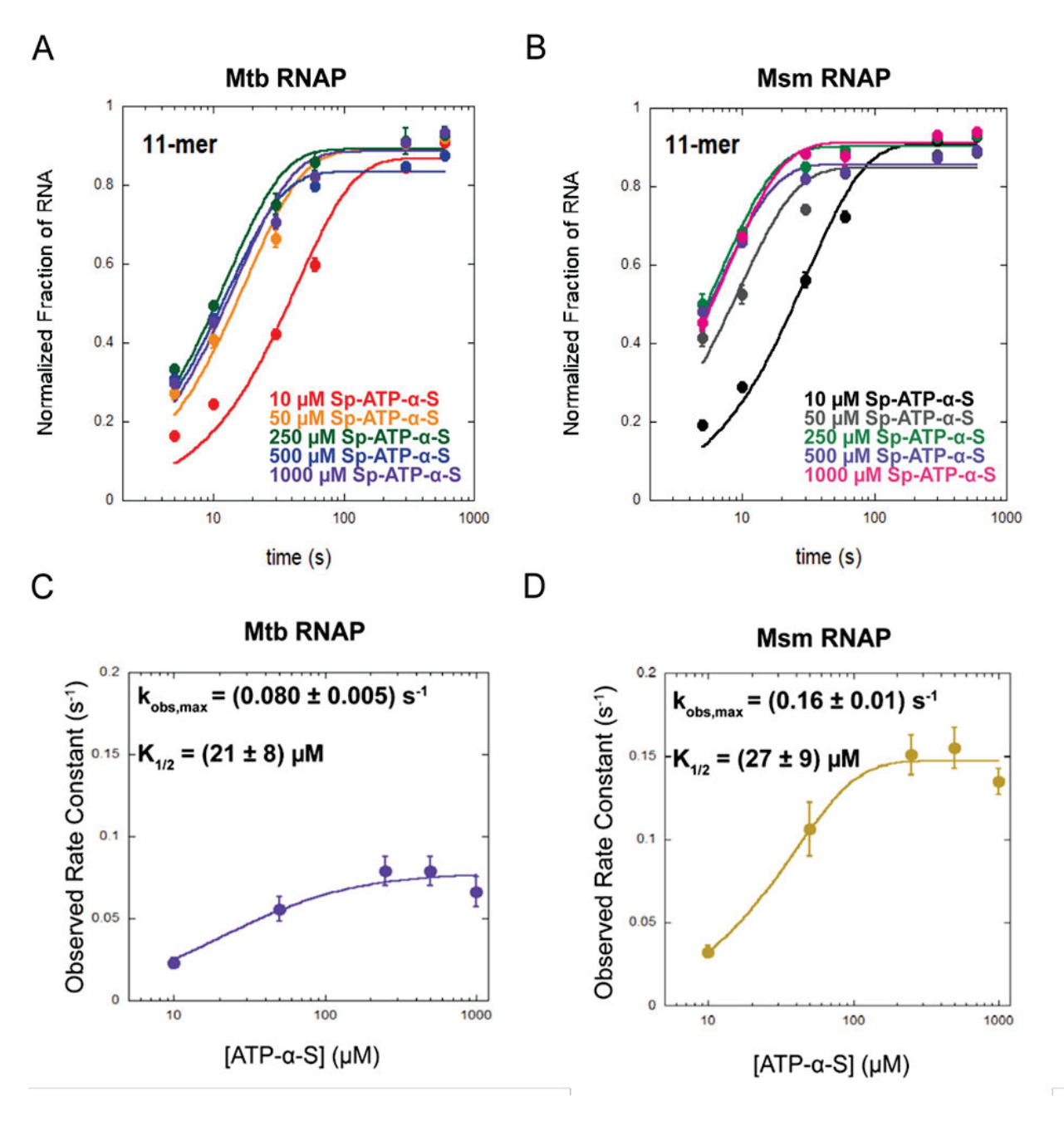


FIG 3 Model-independent analysis of perturbing the rate-limiting step by addition of Sp-ATP- $\alpha$ -S. (A) Primary plot of Mtb RNAP-catalyzed Sp-ATP- $\alpha$ -S addition fits to equation 2. (C) Secondary plot of Sp-ATP- $\alpha$ -S addition catalyzed by Mtb RNAP, with calculated parameter values. (D) Secondary plot of Sp-ATP- $\alpha$ -S addition catalyzed by Msm RNAP, with calculated parameter values. Data points represent the average of three experimental replicates, and the error bars represent SD.

a decrease in the maximal observed rate constant by 180-fold when ATP is replaced with Sp-ATP- $\alpha$ -S (Fig. 2C and 3C; Tables S2.1 and S2.2). The  $k_{\rm obs,max,Sp-ATP-\alpha-S} = (0.080 \pm 0.005)$  $s^{-1}$ . These results suggest that bond formation is rate-limiting.

By introducing the slowly hydrolyzable nucleotide analog, the two partially rate-limiting steps we observed during ATP addition are collapsed into a single rate-limiting step describing bond formation. These data suggest that an isomerization of inactive to active complexes is no longer partially rate-limiting at sufficient [ATP].

Interestingly, we also observed a 7.7-fold decrease in the  $K_{1/2}$  upon the addition of Sp-ATP- $\alpha$ -S (Fig. 3C; Tables S1.2 and S2.2) compared to ATP. Mtb RNAP  $K_{1/2}$  for ATP = (162  $\pm$  73)  $\mu$ M, whereas the  $K_{1/2}$  for Sp-ATP- $\alpha$ -S = (21  $\pm$  8)  $\mu$ M (Fig. 2C and 3C; Tables S1.2 and S2.2). This significant decrease in both  $k_{\rm obs,max}$  and  $K_{1/2}$  was not observed for nucleotide addition by eukaryotic Pol II, using the same experimental design (21). This result suggests that Mtb RNAP binds the nucleotide analog with higher affinity than canonical ATP. The significant difference between Mtb RNAP and Pol II Sp-ATP-α-S addition potentially results from the structural differences observed in the subunit composition of these enzymes (2, 8). We hypothesize that Mtb RNAP may demonstrate sensitivity to nucleotide analogs in vivo, providing a potential target for inhibition of the bacterial pathogen.

We performed the same experiments of ATP and Sp-ATP- $\alpha$ -S addition using Msm RNAP and observed similar results to Mtb RNAP (Fig. 2B and 3B; Tables S1.1 and S2.1). Msm RNAP-catalyzed addition demonstrated a 125-fold decrease in maximum observed rate constant (Fig. 2D and 3D; Tables S1.2 and S2.2). For ATP addition,  $k_{\rm obs,max}$  = (20  $\pm$ 1.6) s<sup>-1</sup>. For Sp-ATP- $\alpha$ -S,  $k_{\text{obs,max,Sp-ATP-}\alpha$ -S} = (0.16 ± 0.01) s<sup>-1</sup> (Fig. 2D and 3D; Tables S1.2 and S2.2). Additionally, a ninefold decrease of  $K_{1/2}$  was observed,  $K_{1/2}$  for ATP = (243  $\pm$ 58)  $\mu$ M, whereas the  $K_{1/2}$  for Sp-ATP- $\alpha$ -S = (27  $\pm$  9)  $\mu$ M (Fig. 2D and 3D; Tables S1.2, S2.2). These results suggest that Mtb RNAP and Msm RNAP demonstrate similar sensitivity to nucleotide analogs, unlike eukaryotic Pol II (21).

## Model-dependent analysis of single nucleotide addition using the MATLAB tool MENOTR

To characterize the mechanism of nucleotide addition, we employed the custom built MATLAB tool Multi-start Evolutionary Nonlinear OpTimizeR (MENOTR) to determine the kinetic mechanism describing nucleotide addition by Mtb RNAP and Msm RNAP (26). This tool uses a combination of genetic algorithm and NLLS to determine the best fit parameters for each kinetic step defined by the kinetic mechanism (scheme) provided (19-21, 23-26).

Many kinetic schemes were tested, and the simplest scheme we determined to fit the time courses is presented as Scheme 1 (Fig. 4A; Fig. S1 to S3). The other, more straightforward schemes did not describe the data well and presented systematic deviation between the fit and data points (Fig. S1 to S3). The best-fitting scheme we determined requires two populations of ECs (EC<sub>10</sub> and EC<sub>10</sub>-ATP). These populations describe two ATP-binding events. The first between EC<sub>10</sub> and ATP, the second between EC<sub>10</sub>-bound to ATP with another ATP-binding event (Fig. 4A). Most interestingly, both EC populations are sensitive to the [ATP] present, resulting in bimolecular rate constants describing the first two steps in the reaction scheme. The following step describes bond formation, extension of the nascent RNA to an 11-mer, and release of pyrophosphate (PPi).

With our experimental design, we are only sensitive to rate-limiting steps and are not able to deconvolute very fast kinetic steps; because of this, we hypothesize that within the reversible kinetic steps, described by elementary rate constants, fast conformational changes and PPi release are occurring, but these cannot be measured with this experimental design (19-22). Global fitting of nucleotide addition catalyzed by Mtb RNAP at five [ATP] is presented in Fig. 4B, with corresponding rate constants (k) provided in Table 1. At the bottom of each table is the  $X^2$  value, the measure of goodness of fit. The parallel study of Msm RNAP using the same experimental design is presented

## Scheme 1

$$EC_{10} + ATP \xrightarrow{k_1 \atop k_2} (EC_{10} \bullet ATP) + ATP \xrightarrow{k_3 \atop k_4} EC_{10} \bullet ATP_2 \xrightarrow{k_5 \atop k_6} EC_{11} + PP$$

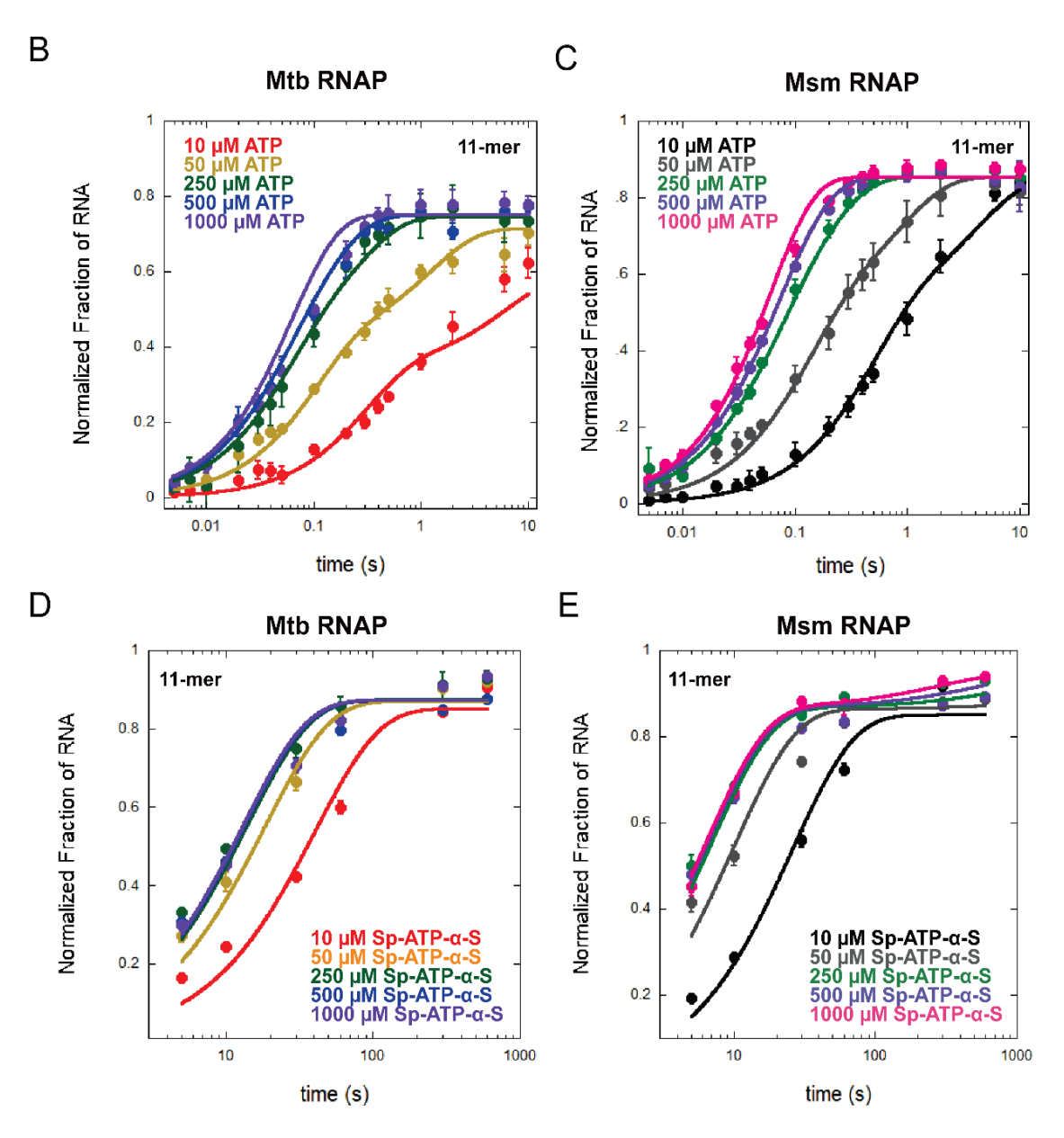


FIG 4 Model-dependent analysis of single nucleotide addition time courses. (A) Scheme 1 describes the kinetic mechanism of nucleotide addition for both Mtb RNAP and Msm RNAP. (B) Global model-dependent fitting using Scheme 1 in MENOTR for ATP addition catalyzed by Mtb RNAP. Individual parameters with upper and lower bounds are listed in Table 1. (C) Global model-dependent fitting of ATP addition catalyzed by Msm RNAP. Parameter values are listed in Table 2. (D) Global model-dependent fitting using Scheme 1 in MENOTR for Sp-ATP-α-S addition catalyzed by Mtb RNAP. Parameter values are listed in Table 3. (E) Global model-dependent fitting using Scheme 1 in MENOTR for Sp-ATP-α-S addition catalyzed by Msm RNAP. Parameter values are listed in Table 4. Data points represent the average of three experimental replicates, and error bars represent the SD.

TABLE 1 Global fitting of Mtb RNAP-catalyzed ATP addition<sup>a</sup>

Elementary rate constant	Mtb RNAP	Lower bound	Upper bound
$(s^{-1})$	ATP		
$\overline{k_1}$	18121.7	10980.9	29282.3
k <sub>2</sub>	3.88	2.70	7.21
k <sub>3</sub>	1e + 8	_	-
k <sub>4</sub>	13298.8	9567.8	20010.3
k <sub>5</sub>	16.03 <sup>b</sup>	12.72	17.94
k <sub>6</sub> X <sup>2</sup>	0.40	0.20	0.50
$\chi^2$	0.0820		

<sup>&</sup>lt;sup>a</sup>X<sup>2</sup> values represent goodness of fit.

in Fig. 4C, with calculated rate constants presented in Table 2. We highlight k5 as the rate constant governing bond formation in each table.

## Model-dependent analysis of Sp-ATP-α-S incorporation using MENOTR

We used the same kinetic scheme to define the parameter values of Sp-ATP- $\alpha$ -S addition for both Mtb RNAP and Msm RNAP. Our results are in agreement with the model-independent analysis revealing the approximately 100-fold decrease in the elementary rate constants ( $k_5$ ) describing bond formation for both RNAPs (Fig. 4D and E; Tables 3 and 4). These analyses further reinforce our hypothesis that we are observing two populations of ECs, both of which demonstrate bond formation as the rate-limiting step.

## Model-dependent analysis of multiple nucleotide addition events catalyzed by Mtb RNAP

In vivo, RNAPs perform RNA synthesis by adding tens to thousands of nucleotides to form nascent RNA (27, 28). To better characterize transcription elongation beyond a single nucleotide addition event, we employed the previously described in vitro transcription experiment with one alteration; the addition of GTP as well as ATP. Based upon the template DNA sequence, the nascent RNA synthesized will extend from a radiolabeled 10-mer to a final 19-mer RNA with the sequence 5'-AUCGAGAGGCAGGAGGAA-3'. RNA species of defined lengths are separated via PAGE, and the signal intensity of each intermediate is quantified and normalized to the starting 10-mer RNA signal. We then performed a model-dependent analysis of multi-nucleotide addition time courses using Scheme 2 (Fig. 5A). Scheme 2 defines forward and reverse rate constants for the formation of each RNA intermediate as well as the final RNA product (Fig. 5B through E; Fig. S4). The k<sub>obs</sub> values for each rate constant were calculated for time courses catalyzed by both Mtb RNAP and Msm RNAP (Tables 5 and 6). We again see the similarity in the average observed rate constants for both RNAPs across nine nucleotide additions. Mtb RNAP average =  $(22.1 \pm 17.5)$  s<sup>-1</sup>. Msm RNAP is consistently slightly faster, with average =  $(24.2 \pm 18.7) \text{ s}^{-1}$ .

TABLE 2 Global fitting of Msm RNAP-catalyzed ATP addition<sup>a</sup>

Elementary rate constant	Msm RNAP	Lower bound	Upper bound
(s <sup>-1</sup> )	ATP		
k <sub>1</sub>	24663.3	15930.7	31134.1
$k_2$	25.34	13.18	35.14
k <sub>3</sub>	1e + 8	-	-
k <sub>4</sub>	12780.9	8525.5	14150.7
k <sub>5</sub>	25.85 <sup>b</sup>	23.98	31.57
k <sub>6</sub>	0.001	0.0010	0.0011
$\chi^2$	0.0581		

 $<sup>{}^{</sup>a}X^{2}$  values represent goodness of fit.

<sup>&</sup>lt;sup>b</sup>k3 is fixed at the diffusion limit, without lower or upper bounds.

bk3 is fixed at the diffusion limit, without lower or upper bounds.

**TABLE 3** Global fitting of Mtb RNAP-catalyzed Sp-ATP-α-S addition<sup>a</sup>

Elementary rate constant	Mtb RNAP	Lower bound	Upper bound
(s <sup>-1</sup> )	ATP-α-S		
k <sub>1</sub>	3.47	1.89	5.05
$k_2$	0.010	0.005	0.015
k <sub>3</sub>	1e + 8	-	_
k <sub>4</sub>	3364.16	2335.09	4742.84
k <sub>5</sub>	0.164 <sup>b</sup>	0.145	0.195
k <sub>6</sub>	0.001	0.001	0.001
$\chi^2$	0.0417		

<sup>&</sup>lt;sup>a</sup>X<sup>2</sup> values represent goodness of fit.

The analysis of multiple nucleotide addition events again reveals conservation between Mtb RNAP and Msm RNAP. Despite the pathogenic differences between these mycobacterial species, we observe similar nucleotide addition characteristics of these Actinobacteria (8). How these observed nucleotide addition kinetics for multiple nucleotide addition events compare to other bacterial RNAPs remains to be elucidated.

Previously, our lab has used a similar promoter-independent in vitro transcription method to characterize multiple nucleotide addition events catalyzed by the eukaryotic Pols I, II, and III, at single-nucleotide resolution (19, 20). Comparing enzymes of similar function but diverse evolution, we observe fundamental differences and similarities in the mechanisms of nucleotide addition catalyzed by bacterial vs eukaryotic RNA polymerases.

In this study, we observe that Mtb RNAP and Msm RNAP demonstrate reversibility at each intermediate during multiple nucleotide addition events (Fig. 5A). Recent studies observed this same requirement of reversibility for eukaryotic Pol II and ΔA12.2 Pol I but not WT Pol I or Pol III (Fig. 5A) (19, 20, 23, 24). ΔA12.2 Pol I lacks the bona fide exonuclease subunit, and Pol II was not provided TFIIS in these studies, suggesting that lacking intrinsic nuclease activity results in PPi remaining in close proximity to the recently added NTP (23, 24).

#### **EC** stability

In addition to the mechanism by which nucleotide addition occurs, a critical property of transcription elongation is the stability of the ECs (19). ECs must be stable enough to allow for processive transition between bond formation steps but not so stable as to prevent disengagement of the RNAP at termination sites (19-22, 27). In vivo, specific sets of transcription factors participate in regulation of transcription initiation, elongation, and termination (10-13). In our minimal RNAP-only in vitro system, we evaluate the fundamental stability of the RNAP assembled in an active elongation complex over time.

To test the stability of ECs formed with Mtb RNAP and Msm RNAP, we employed an RNase A protection experiment (19, 25). We performed the same EC assembly steps

TABLE 4 Global fitting of Msm RNAP-catalyzed Sp-ATP-α-S addition<sup>a</sup>

Elementary rate constant	Msm RNAP	Upper bound	Lower bound
(s <sup>-1</sup> )	ATP-α-S		
k <sub>1</sub>	1.26	0.69	1.83
$k_2$	0.006	0.005	0.009
k <sub>3</sub>	1e + 8	_	_
k <sub>4</sub>	2221.45	1366.21	3231.20
k <sub>5</sub>	$0.080^{b}$	0.068	0.096
k <sub>6</sub>	0.001	0.001	0.001
$\chi^2$	0.0585		

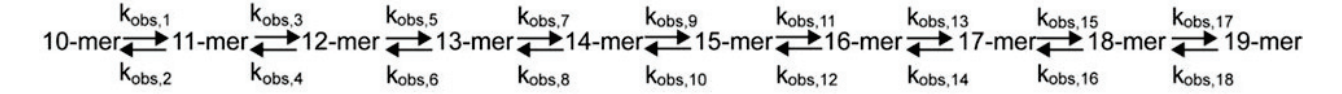
 $<sup>{}^{</sup>a}X^{2}$  values represent goodness of fit.

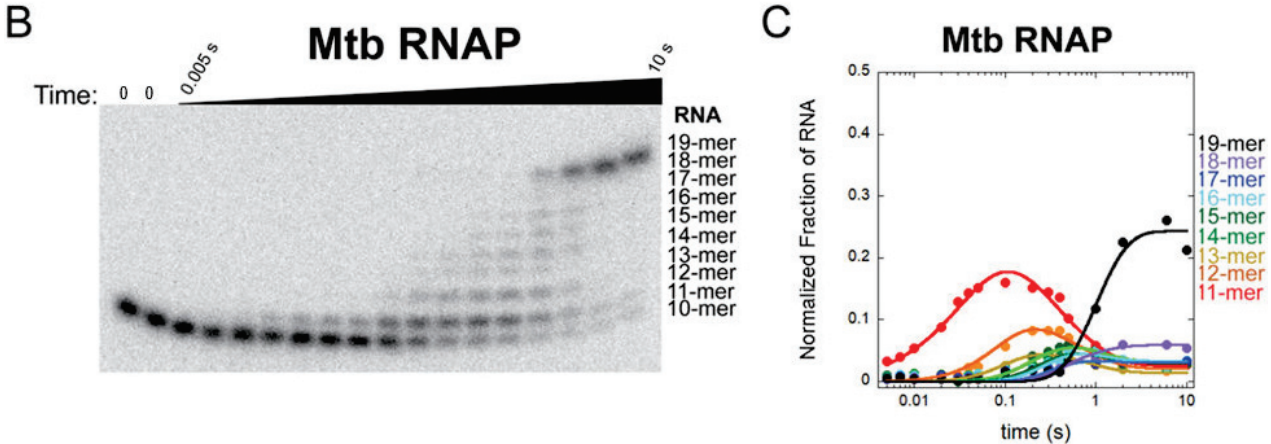
<sup>&</sup>lt;sup>b</sup> k3 is fixed at the diffusion limit, without lower or upper bounds.

bk3 is fixed at the diffusion limit, without lower or upper bounds.

Journal of Bacteriology

## Scheme 2





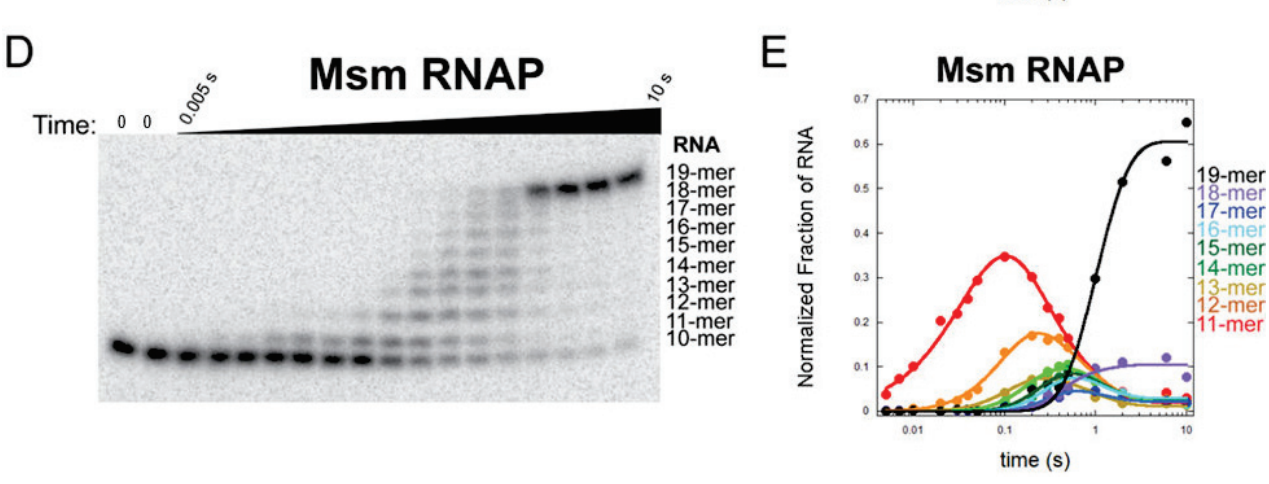


FIG 5 Model-dependent analysis of multi-nucleotide addition catalyzed by Mtb RNAP or Msm RNAP. (A) Scheme 2 defines the kinetic mechanism of nine sequential nucleotide addition events catalyzed by Mtb RNAP or Msm RNAP. (B) Representative gel image of multi-nucleotide addition catalyzed by Mtb RNAP. (C) Representative global fitting of one replicate of Mtb RNAP nucleotide addition performed using MENOTR. Parameter values are listed in Table 5. (D) Representative gel image of multi-nucleotide addition catalyzed by Msm RNAP. E) Representative global fitting of one replicate of Msm RNAP nucleotide addition using MENOTR. Parameter values are listed in Table 6.

as described above; pre-binding the RNAP to an annealed RNA:DNA hybrid, providing the non-template DNA strand to form an active complex, and radiolabeling with the addition of  $\alpha$ - $^{32}$ P-CTP. After halting the labeling reaction, we subjected the ECs to a destabilizing salt solution and RNase A, which will cleave the RNA following unpaired pyrimidine residues (19). If the EC is intact at the time the sample is collected, the RNA is protected from RNase activity, and a full-length 10-mer RNA will be visualized. If the EC has collapsed by the time a sample is collected, the RNA is exposed to RNase A cleavage, and a shorter 7-mer RNA will be visualized (Fig. 6A). We then quantify the proportion of EC collapse over time (Fig. 6B).

From these EC stability experiments, we determined that Mtb RNAP and Msm RNAP form similarly stable complexes, with approximately 50% collapse within 5 hours and the

Downloaded from https://journals.asm.org/journal/jb on 03 July 2025 by 138.26.72.87.

TABLE 5 Calculated rate constants for Mtb RNAP multi-nucleotide addition<sup>a</sup>

Observed rate constant	Mtb RNAP	SD
$(s^{-1})$	1 mM ATP	
	1 mM GTP	
k <sub>obs,1</sub>	8.50	3.08
$k_{\text{obs,2}}$	5.84	3.75
$k_{\text{obs,3}}$	7.58	4.60
$k_{\text{obs,4}}$	10.9	6.32
k <sub>obs,5</sub>	26.2	7.99
k <sub>obs,6</sub>	50	0
k <sub>obs,7</sub>	22.2	4.41
k <sub>obs,8</sub>	10	0
$k_{\text{obs,9}}$	41.3	4.30
k <sub>obs,10</sub>	50	0
k <sub>obs,11</sub>	51.9	2.54
k <sub>obs,12</sub>	50	0
k <sub>obs,13</sub>	14.5	6.91
k <sub>obs,14</sub>	14.1	9.03
k <sub>obs,15</sub>	17.3	1.17
k <sub>obs,16</sub>	8.02	2.56
k <sub>obs,17</sub>	7.99	1.68
k <sub>obs,18</sub>	1.72	0.46
$\chi^2$	0.0136	

 $<sup>^{\</sup>it a}{\it X}^{\it 2}$  values represent goodness of fit.

majority of ECs having collapsed by 12 hours (Fig. 6B). This is another area of significant deviation from eukaryotic Pol II, which forms ECs that are stable on the order of days under similar experimental conditions (19). These results are also unique as compared to ECs formed by eukaryotic Pol II, which demonstrate total collapse by 40 min and eukaryotic Pol III, which demonstrate near total collapse by 3.5 hours (19, 20). The results

TABLE 6 Calculated rate constants for Msm RNAP multi-nucleotide addition<sup>a</sup>

Observed rate constant	Msm RNAP	SD	
(s <sup>-1</sup> )	1 mM ATP		
	1 mM GTP		
k <sub>obs,1</sub>	11.4	1.23	
$k_{\text{obs,2}}$	4.93	1.51	
$k_{\text{obs,3}}$	10.2	0.82	
$k_{\text{obs,4}}$	6.67	4.55	
k <sub>obs,5</sub>	33.0	17.27	
$k_{\text{obs,6}}$	56.0	44.78	
k <sub>obs,7</sub>	28.2	6.28	
$k_{\text{obs,8}}$	14.3	4.61	
$k_{obs,9}$	24.2	8.10	
$k_{\text{obs,10}}$	20.3	9.89	
k <sub>obs,11</sub>	53.2	7.19	
$k_{\text{obs,12}}$	50	0	
$k_{\text{obs,13}}$	46.4	11.98	
$k_{\text{obs,14}}$	50	0	
k <sub>obs,15</sub>	15.6	2.60	
k <sub>obs,16</sub>	3.41	2.20	
k <sub>obs,17</sub>	6.37	3.07	
k <sub>obs,18</sub>	1.15	0.53	
$\chi^2$	0.0137		

 $<sup>^{</sup>a}X^{2}$  values represent goodness of fit.

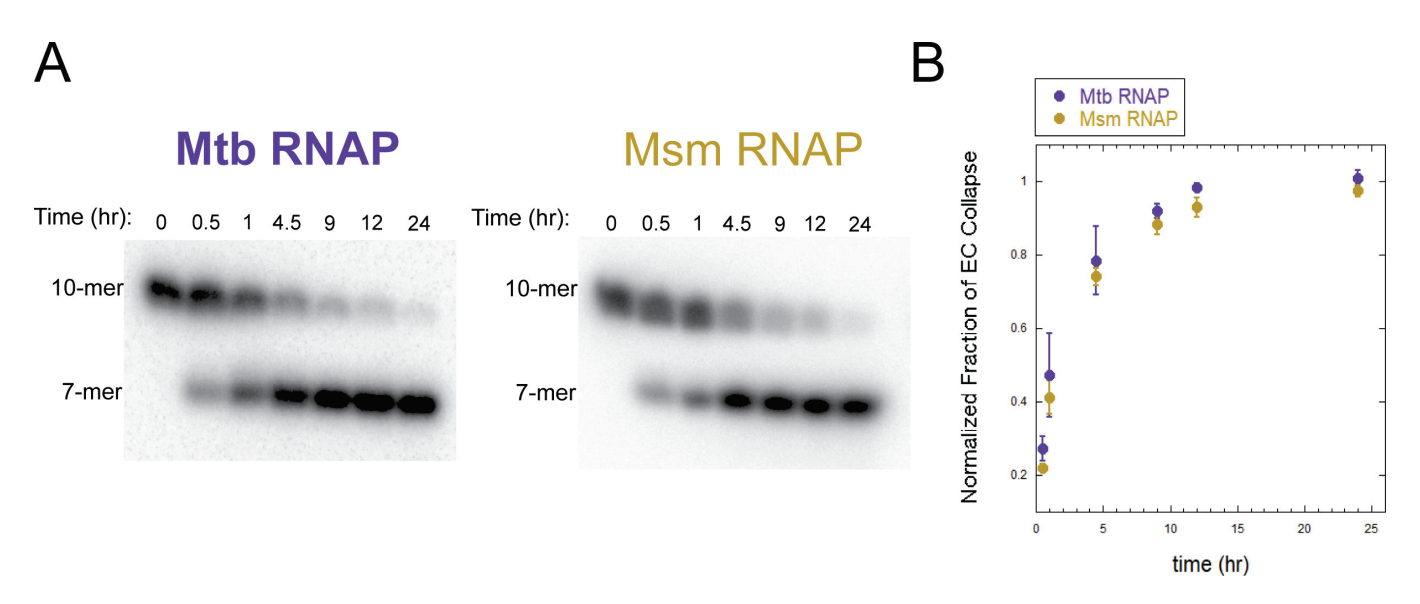


FIG 6 Elongation complex stability time courses of complexes formed with either Mtb RNAP or Msm RNAP. (A) Representative gel images of EC stability time courses of Mtb RNAP and Msm RNAP. Time points are listed in minutes at the top of each image. (B) Plotted EC stability time courses of Mtb RNAP and Msm RNAP over the duration of 24 hours. Data points represent the average of three experimental replicates, and error bars represent the SD.

of these experiments highlight the distinct enzymatic properties of RNAPs (and Pols) from different domains of life. While the function of RNA synthesis is conserved, the intrinsic properties of each enzyme differ widely.

# Model-independent evaluation of *E. coli* RNAP single nucleotide addition at low and high [ATP]

In this study, we observed substantial deviation between the mechanisms of nucleotide addition by *Mycobacterial* RNAP and the eukaryotic Pols. These differences were obvious even in the model-independent analysis of single nucleotide addition catalyzed by Mtb

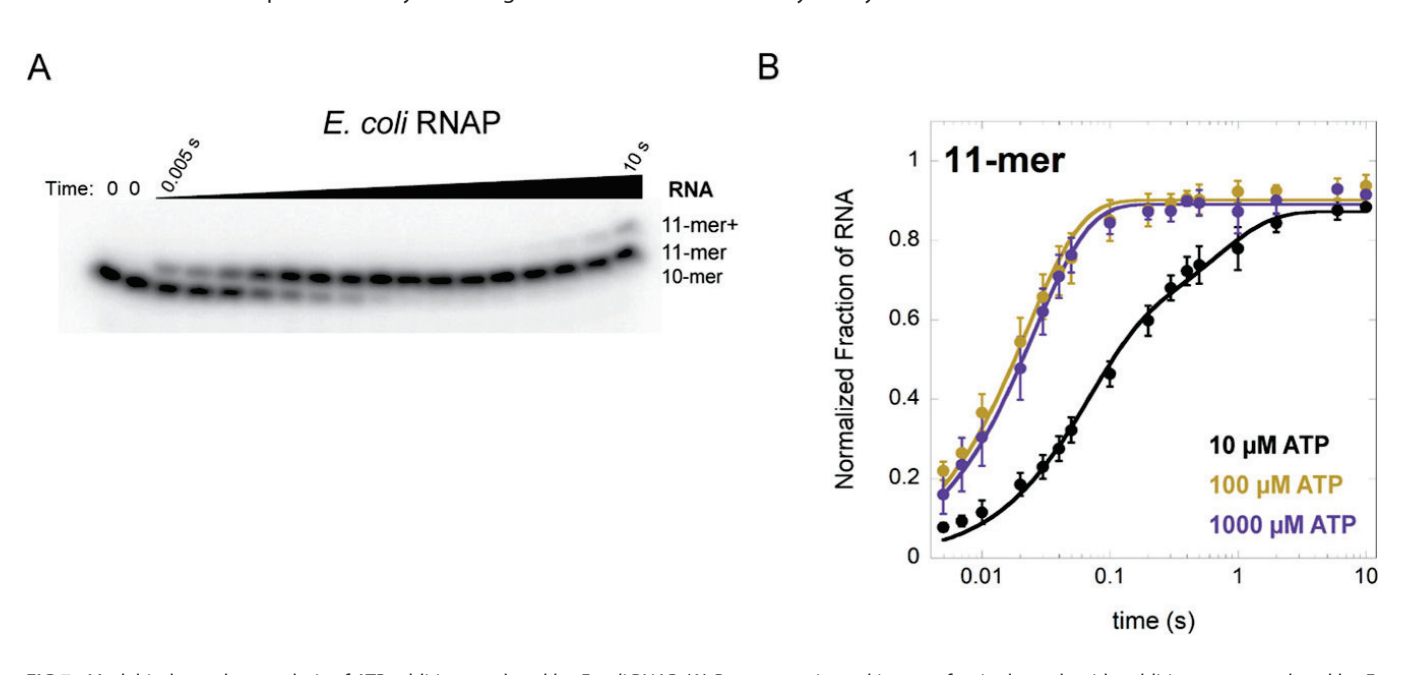


FIG 7 Model-independent analysis of ATP addition catalyzed by *E. coli* RNAP. (A) Representative gel image of a single nucleotide addition event catalyzed by *E. coli* RNAP over time. (B) Plot of *E. coli* RNAP-catalyzed ATP addition. Ten micromolar ATP data is fit to equation 1, ≥100 μM ATP data are fit to equation 2. Data points represent the average of three experimental replicates, and error bars represent the SD. Fitting of 10 μM, 100 μM, and 1,000 μM data all fit equation 2 is presented in Fig. S4.

RNAP and Msm RNAP (Fig. 2). To describe the data using model-dependent analysis, we used a unique and complex kinetic scheme (Fig. 4A; Fig. S1 to S3). This scheme is unlike any our lab has previously used to describe nucleotide addition catalyzed by eukaryotic Pols (19–22). This observation led to the question: is this unusual mechanism specific to *Mycobacterial* RNAPs, or is it perhaps conserved among other bacterial RNAPs?

Studies performed by the Erie lab have previously provided insight into a complex mechanism of nucleotide addition catalyzed by *E. coli* RNAP (6, 29). To test for conservation of an [ATP]-dependent, biphasic mechanism of nucleotide addition, we performed single nucleotide addition experiments catalyzed by *E. coli* RNAP at multiple [ATP] (Fig. 7). Model-independent analysis of single nucleotide addition catalyzed by *E. coli* RNAP is presented in Fig. 7, with parameter values listed in Table S3. As observed for Mth RNAP

mechanism of nucleotide addition catalyzed by *E. coli* RNAP (6, 29). To test for conservation of an [ATP]-dependent, biphasic mechanism of nucleotide addition, we performed single nucleotide addition experiments catalyzed by *E. coli* RNAP at multiple [ATP] (Fig. 7). Model-independent analysis of single nucleotide addition catalyzed by *E. coli* RNAP is presented in Fig. 7, with parameter values listed in Table S3. As observed for Mtb RNAP and Msm RNAP, time courses collected with *E. coli* RNAP are best described by a sum of two exponentials at low [ATP] but a single exponential at high [ATP] (Fig. 2A, B and 7B; Tables S1.1 and S3.1; Fig. S5). This observation is consistent with the [ATP]-dependent shift in nucleotide addition kinetics being conserved between *Mycobacteria* and *E. coli*. Future experiments will investigate the detailed kinetic mechanism of nucleotide addition catalyzed by *E. coli* RNAP.

#### DISCUSSION

# Mtb RNAP and Msm RNAP are enzymatically similar and divergent from eukaryotic Pols

Much of our understanding of transcription in bacteria comes from studies in model systems, such as *E. coli, Bacillus subtilis*, and *Thermus* species (1–6, 29–36). In recent years, it has been appreciated that *Mycobacterial* species display significant divergence from the established model systems with regard to the roles of trans-acting factors, the kinetics of transcription, as well as structural interactions with therapeutic molecules (10–17, 36, 37). In this study, we investigated the unique enzymatic features of Mtb RNAP with comparison to the related lab-safe strain Msm RNAP. With our results, we also consider how these two bacterial RNAPs are similar and divergent from eukaryotic RNA polymerases (Pols).

Using our established *in vitro* transcription elongation techniques, we identified the unique kinetic mechanism describing nucleotide addition by Mtb and Msm RNAPs (Fig. 5A). The chemical reaction scheme describing nucleotide addition identifies two populations of ECs, both of which are responsive to the [ATP]. We have previously observed two populations of ECs for eukaryotic Pols, an inactive and an active population, but only the active population was sensitive to [ATP] (19–21). The observed [ATP]-dependence of EC activation may be specific to bacterial RNAPs.

Previous studies have shown that *E. coli* RNAP demonstrated a similar [NTP]-dependent isomerization from a low-activity state to a highly active state, which was reflected by the increased rate of nucleotide addition (6, 29). We have further explored the conservation of the [ATP]-dependent mechanism of nucleotide addition by bacterial RNAPs to include *E. coli* RNAP in this study. We found the same trends at low and high [ATP] for Mtb RNAP, Msm RNAP, and *E. coli* RNAP (Fig. 2A, B and 7B).

In this study, we present the detailed kinetic mechanism that best describes a single nucleotide addition by Mtb RNAP and Msm RNAP (Fig. 4A). This mechanism is fundamentally different from what has been identified for nucleotide addition catalyzed by eukaryotic Pols I, II, and III (19, 20). However, when observing multiple nucleotide addition events, we identified reversibility between RNA intermediates which is consistent with multiple nucleotide addition events catalyzed by Pol II (23). The requirement of reversibility to describe the spread of the rise and fall of each intermediate suggests that pyrophosphorolysis is occurring (Fig. S4) (23). Unlike an irreversible hydrolysis reaction, reversibility requires the presence of PPi in the active site to attack the nucleotide backbone (23, 24). Mtb RNAP and Msm RNAP require additional factors for nuclease activity *in vivo*, similar to Pol II (15–17). The reversibility observed for Pol II,

Mtb RNAP, and Msm RNAP suggests that pyrophosphorolysis occurs in the absence of transacting exonucleolytic factors (21, 23, 24). These findings for Mtb and Msm RNAPs, as well as Pol II, suggest that in the absence of exonuclease activity, pyrophosphorolysis may act as a proofreading mechanism (23).

Previous studies by our lab have characterized the *in vitro* EC stability of eukaryotic Pol I (with and without the A12.2 subunit), Pol II, and Pol III (19, 20, 24, 25). Pol I has been shown to be the least stable, demonstrating the majority of ECs collapse in 40 min (19), Pol III is stable on the order of a few hours (20), and Pol II demonstrates the longest stability over the course of 72 hours (19). Interestingly, our analysis of Mtb RNAP and Msm RNAP EC stability shows that these two mycobacterial RNAPs are similarly stable compared to each other and collapse over the course of 12 hours under our experimental conditions (Fig. 6B). These results suggest that minimal ECs formed with Mtb RNAP or Msm RNAP are more stable than ECs formed with Pol I or Pol III but less stable over time than ECs formed with Pol II, further highlighting the fundamentally different enzymatic properties of RNA polymerases from different domains of life.

Considering the [NTP]-dependent steps determined for the kinetic scheme, we hypothesized that introducing a slowly hydrolyzable nucleotide analog would result in several fold-decrease in the rate constants observed. Our results are consistent with this hypothesis for both Mtb RNAP and Msm RNAP (Fig. 3). We observe a 180-fold decrease in the  $k_{obs,max}$  for Mtb RNAP and a 125-fold decrease in the  $k_{obs,max}$  for Msm RNAP (Fig. 3; Tables S1.2 and S2.2). This significant decrease in the maximum observed rate constant suggest that we are observing bond formation as the primary rate-limiting step.

Interestingly, we also observe a significant decrease in the measure of binding affinity,  $K_{1/2}$ , for both Mycobacterial RNAPs (Fig. 3; Tables S1.2 and S2.2). This finding is significant as it suggests that Mtb RNAP binds nucleotide analogs with significantly higher affinity than canonical nucleotides. Previous studies have suggested that Sp-ATP-α-S more closely mimics the transition state of ATP hydrolysis, resulting in higher binding affinity (38). However, studies performed by our lab show that eukaryotic Pol II does not demonstrate increased affinity for this nucleotide analog (21). Nucleotide analogs have been therapeutically established in the treatments of viral infections and cancer but have not been explored as a method of treatment for tuberculosis (39-44). The success of various FDA-approved nucleotide analogs, such as acyclovir and tenofovir, suggest that the host enzymes are less vulnerable to the effects of the analog in vivo as compared to enzymes of invading pathogenic species (38). These clinical results are consistent with Pol II not binding nucleotide analogs with increased affinity, as Pol II inhibition is lethal and presents a promising strategy to uniquely target Mtb RNAP (40, 41). With the annual increase in the number of drug-resistant tuberculosis cases reported, there is an urgent need for new and effective treatments (7, 45). Future studies will test the effect of established therapeutic nucleotide analogs on the kinetics of nucleotide addition catalyzed by Mtb RNAP.

#### **MATERIALS AND METHODS**

#### Protein expression and purification

Mtb RNAP expression plasmid pMP61, a gift from the Landick lab [University of Wisconsin–Madison (13)], was transformed via electroporation into BL21(DE3)\_Star *E. coli* expression cells and grown in Luria-Bertani (LB) medium supplemented with 50  $\mu$ g/mL kanamycin. Three liter of cell culture in LB + 50  $\mu$ g/mL kanamycin was grown at 37°C with constant shaking at 250 RPM until an OD<sub>600</sub> of 0.65 was reached. Expression was then induced with the addition of 1 mM isopropyl- $\beta$ -D-thiogalactopyranoside (Fisher Scientific, Waltham, MA). Induction was performed for 2 hours at 30°C with constant shaking at 250 RPM. Cells were harvested via centrifugation at 6,000 RPM for 12 min at 4°C then frozen overnight at -80°C.

Frozen cells were resuspended in 100 mL of Lysis Buffer [20 mM Tris-HCl pH 7.8, 5% glycerol (vol/vol), 750 mM KCl, 20 mM imidazole, and 0.5 mM BME

(beta-mercaptoethanol)]. Cells were disrupted via continuous-flow French Press cell disruptor at 25 psi. Crude cell lysate was then separated via ultra-centrifugation at 34,000 RPM for 1 hour at 4°C. Cleared cell lysate was loaded onto  $2 \times 5$  mL HisTrap FF (Ni Sepharose) columns (Cytiva, Marlboroug, MA). Loaded HisTrap columns were washed with Lysis Buffer. Following the wash step, a 1 mL HiTrap Q FF (Q-Sepharose; Cytiva) column was added downstream of the HisTrap columns, and protein was eluted onto Q-Sepharose using Elution Buffer 1 [20 mM Tris-HCl pH 7.8, 5% glycerol (vol/vol), 75 mM KCl, 150 mM imidazole, and 0.5 mM BME].

The Q-Sepharose column was washed with Wash Buffer [20 mM Tris-HCl pH 7.8, 75 mM KCl, 5 mM MgCl<sub>2</sub>, and 10% glycerol (vol/vol)]. Protein was eluted from the Q-Sepharose column via fractionation using Elution Buffer 2 [20 mM Tris-HCl pH 7.8, 2 M KCl, 5 mM MgCl<sub>2</sub>, and 10% glycerol (vol/vol)]. Peak fractions were combined and concentrated using 50,000 MWCO centrifugal filter units (Millipore Sigma, Burlington, MA). Concentrated eluate was further purified and fractionated using size exclusion chromatography via a Superdex 200 Increase 10/300 Gl column (Cytiva) and Sizing Buffer [20 mM Tris-HCl pH 7.8, 200 mM KCl, and 30% glycerol (vol/vol)]. Sizing column elution peaks were fractionated in 1 mL fractions, aliquoted in 250  $\mu$ L fractions, and stored immediately at  $-80^{\circ}$ C.

Purification of Msm RNAP was performed as described above from *E. coli* BL21(DE3)\_Star carrying the expression plasmid pRMS4, a gift from Libor Krásný [Institute of Microbiology of The Czech Academy of Sciences (17)]. Both Mtb RNAP and Msm RNAP expression plasmids, pMP61 and pRMS4, respectively, contain a  $\beta$ - $\beta$ ' subunit fusion for protein stabilization (9, 14, 17).

Purified *E. coli* RNAP was a gift from C. Turnbough, University of Alabama at Birmingham (46).

#### **Buffers**

*In vitro* time course studies were performed in Reaction Buffer: (10 mM Tris-HCl pH 7.8 at 25°C, 20 mM KCl, 0.1 mM dithiothreitol, 0.1 mg·mL<sup>-1</sup> bovine serum albumin); prepared immediately before use from filter sterilized stocks using 0.22 μm Millipore vacuum-driven filters (EMD Millipore, Billerica, MD).

## Oligonucleotides

Template and non-template oligonucleotides and oligoribonucleotide primer were purchased from Integrated DNA Technologies (Coralville, IA). Both template and non-template oligonucleotides were gel purified, then dialyzed against Reaction Buffer. The oligoribonucleotide primer was also dialyzed against Reaction Buffer.

The RNA:DNA hybrid was pre-annealed using thermal cycling, each preparation consisted of 10  $\mu$ M RNA and 3.3  $\mu$ M template DNA.

## Nucleotides

Stocks of ATP and GTP were purchased as 5'-triphosphate disodium salts from Millipore-Sigma (Darmstadt, Germany) and resuspended in reaction buffer. Stock of Sp-ATP- $\alpha$ -S was purchased as disodium salt from Biolog Life Science Institute (Bremen, Germany) and resuspended in reaction buffer. Stocks were then dialyzed against reaction buffer. Concentrations of stock NTP were determined using dual-beam spectrophotometry.

## **Template DNA sequence**

5′–ACCAGCAGGCCGATTGGGATGGGTATTCCCTCCTGCCTCTCGATGGCTGTAAGTATCCTATAG G–3′.

## Non-template DNA sequence

5′-CCTATAGGATACTTACAGCCATCGAGAGGCAGGAGGGAATACCCATCCCAATCGGCCTGCTG GT-3′.

### **RNA** primer sequence

5'-AUCGAGAGG-3'.

## Rapid mixing time courses

Single nucleotide addition time courses catalyzed by Mtb RNAP or Msm RNAP were performed by the addition of either RNAP to Reaction Buffer, followed by the addition of the pre-annealed RNA:DNA hybrid. The RNAP was incubated with the RNA:DNA hybrid on ice for 10 min followed by 10 min at ambient temperature. The non-template DNA was then added and incubated at ambient temperature for 10 min to form an active elongation complex.

Following elongation complex formation, labeling is performed by adding magnesium and  $\alpha$ - $^{32}$ P-CTP. The radiolabeled CTP is incorporated as the next cognate nucleotide and forms visualizable RNA products. The labeling reaction is halted by the addition of EDTA.

Radiolabeled elongation complexes are loaded into one syringe of the chemical quench flow. In the opposite syringe is the NTP solution containing [ATP], or 1 mM ATP and 1 mM GTP for multi-nucleotide addition time courses, along with heparin. Heparin serves as a trap for unbound RNAPs, resulting in single-turnover reaction conditions (15–18). The two solutions are rapidly mixed in 2 ms, and discontinuous time points are collected as  $\Delta t \geq 5$  ms. The reaction is terminated by the rapid addition of 1 M HCl. Collected time points are then neutralized, and the sample is added to formamide dye for storage. Single and multi-nucleotide addition time courses were performed at 25°C.

Time course samples are loaded into 28% acrylamide sequencing gels to separate products from reactants via PAGE. The gels are then exposed to a phosphorimaging screen for at least 12 hours. Imaging of the radiolabeled RNA products is performed using phosphorimaging via the Amersham Typhoon (Cytiva).

## Sp-ATP-α-S addition time courses

Nucleotide addition time courses using the slowly hydrolyzable nucleotide analog Sp-ATP- $\alpha$ -S were performed using the same EC formation steps as previously described as well as the addition of  $\alpha^{-32}$ P-CTP. Following the labeling step, active ECs complexed with either Mtb RNAP or Msm RNAP were mixed by hand with NTP solution containing [Sp-ATP- $\alpha$ -S] and heparin. Time course samples were incubated at 25°C for the duration of the reaction and quenched by hand using formamide dye. Samples were resolved via PAGE as previously described.

#### Data analysis

Gel images are then quantified using ImageQuant software (Cytiva). Pixel intensity of each RNA species is quantified and normalized to the starting material, as described previously in detail (18). The normalized values for each RNA species are initially plotted for model-independent analysis using KaleidaGraph (Synergy Software, Reading, PA).

The model-independent analysis of a single nucleotide addition catalyzed by both Mtb RNAP and Msm RNAP revealed a difference between lower [ATP] and [ATP]  $\geq$ 250  $\mu M$ . Time courses of 10  $\mu M$  ATP and 50  $\mu M$  fit to the sum of two exponentials (equation 1), while time courses of 250  $\mu M$ , 500  $\mu M$ , and 1,000  $\mu M$  fit to a single exponential (equation 2). This result suggested the presence of a partially rate-limiting step that is no longer rate-limiting at sufficient [ATP].

### Model-dependent analysis of single nucleotide addition

To define the kinetic mechanism of a single nucleotide addition at varying [ATP] and varying [Sp-ATP- $\alpha$ -S] by both Mtb RNAP and Msm RNAP, we employed the custom-built MATLAB toolbox MENOTR (19–26). This analysis tool uses a combination of genetic algorithm and NLLS to optimize parameter identification (26). The kinetic mechanism is written as a scheme (Fig. 4A), and each parameter is described using ordinary differential equations.

MENOTR performs simulations to determine the best fit parameters given the experimental data points and defined scheme. Using the combination of NLLS and genetic algorithm, it samples parameters within defined upper and lower limits. Through permutations of random sampling, it defines the best fit parameters for each species identified in the kinetic scheme producing parameter values as well as an  $X^2$  value of the goodness of fit. Upper and lower bounds were determined using grid searching in MATLAB. Determination of the error space was performed using an F-critical value of 1.117.

#### Model-dependent analysis of multi-nucleotide addition

MENOTR was also used to define the kinetic mechanism of multi-nucleotide addition at 1 mM ATP and 1 mM GTP. For both Mtb RNAP and Msm RNAP, a scheme was used that includes reversibility at each nucleotide incorporation step (Fig. 5A). Without reversibility, the best fit lines are not able to describe how intermediates in the multi-nucleotide addition time courses persist in time (23, 24). Using this scheme, parameters for individual replicates were globally optimized. The average parameter values of the replicates with SD are shown in Tables 5 and 6.

Although the reversible scheme described the time courses well, certain observed rate constants floated to values larger than what is detectable by the chemical quench flow. For Mtb RNAP, observed rate constants 5 through 12 exhibited this, while Msm RNAP showed this for observed rate constants 11 through 14. It has been previously shown that sampling the error space for the reverse rate constants via grid searching can detect a lower limit that the parameter can be constrained to without changing the quality of the fit (24). The lower limits were determined for the reverse rate constants for Mtb RNAP and Msm RNAP that floated to large values, and the subsequent global parameter optimizations constrained these reverse rate constants to their respective lower limits. The constrained reverse rate constants are denoted in Tables 5 and 6 as having no associated SD.

## EC stability assay

To determine the time required for ECs to collapse, we employed an RNase protection assay. Evaluation of EC stability for complexes of both Mtb RNAP and Msm RNAP was performed as previously described (15). Briefly, ECs were formed using the same steps as for nucleotide addition time courses, including the incorporation of  $\alpha$ -32P-CTP, but no additional NTPs are provided in the solution. Instead, the labeled ECs are subjected to a destabilizing KCl solution and RNase A, which cleaves RNA at a specific sequence, between cytosine and guanine bases. Intact ECs are protected from RNase A activity, resulting in a full-length 10-mer RNA product. Collapsed ECs allow RNase A activity to cleave the unbound RNA, resulting in an unlabeled 3-mer and a radiolabeled 7-mer RNA product. These two products are quantified to calculate the proportion of EC collapse over time.

#### **ACKNOWLEDGMENTS**

We thank the Krasny and Landick labs for sharing the expression plasmids for Msm and Mtb RNAP, respectively. Their help was critical to the study. We also thank members

of the Schneider and Lucius labs for critical evaluation of the data and suggestions throughout the project.

This work was funded by grants NIH R35 GM140710 to D.A.S., and NSF MCB2346165 to A.L.L. and D.A.S.

#### **AUTHOR AFFILIATIONS**

<sup>1</sup>Department of Biochemistry and Molecular Genetics, Heersink School of Medicine, University of Alabama at Birmingham, Birmingham, Alabama, USA

<sup>2</sup>Department of Chemistry, University of Alabama at Birmingham, Birmingham, Alabama, USA

#### **AUTHOR ORCIDs**

Stephanie L. Cooper (10) http://orcid.org/0000-0001-9928-002X

Aaron L. Lucius (10) http://orcid.org/0000-0001-8636-5411

David A. Schneider (10) http://orcid.org/0000-0003-0635-5091

#### **FUNDING**

Funder	Grant(s)	Author(s)
HHS   NIH   National Institute of General Medical Sciences (NIGMS)	GM140710	David A. Schneider
National Science Foundation (NSF)	MCB2346165 Aaron L. Lucius	
		David A. Schneider

#### **AUTHOR CONTRIBUTIONS**

Stephanie L. Cooper, Conceptualization, Data curation, Formal analysis, Investigation, Validation, Visualization, Writing – original draft, Writing – review and editing | Ryan M. Requijo, Data curation, Formal analysis, Investigation, Writing – review and editing | Aaron L. Lucius, Formal analysis, Funding acquisition, Project administration, Supervision, Writing – review and editing | David A. Schneider, Conceptualization, Data curation, Funding acquisition, Project administration, Supervision, Writing – review and editing

#### **ADDITIONAL FILES**

The following material is available online.

#### Supplemental Material

**Supplemental material (JB00256-24-s0001.docx).** Supplemental figures and tables.

#### **REFERENCES**

- Chan C, Landick R. 1994. New perspectives on RNA chain elongation and termination by *E. coli* RNA polymerase, p 297–321. In Transcription: mechanisms and regulation. R. C. Conaway (New York: Raven Press).
- Sekine S, Tagami S, Yokoyama S. 2012. Structural basis of transcription by bacterial and eukaryotic RNA polymerases. Curr Opin Struct Biol 22:110–118. https://doi.org/10.1016/j.sbi.2011.11.006
- Mustaev A, Roberts J, Gottesman M. 2017. Transcription elongation. Transcription 8:150–161. https://doi.org/10.1080/21541264.2017. 1289294
- L B Almeida B, M Bahrudeen MN, Chauhan V, Dash S, Kandavalli V, Häkkinen A, Lloyd-Price J, S D Cristina P, Baptista ISC, Gupta A, Kesseli J, Dufour E, Smolander OP, Nykter M, Auvinen P, Jacobs HT, M D Oliveira S, S Ribeiro A. 2022. The transcription factor network of *E. coli* steers global responses to shifts in RNAP concentration. Nucleic Acids Res 50:6801– 6819. https://doi.org/10.1093/nar/gkac540
- Weng X, Bohrer CH, Bettridge K, Lagda AC, Cagliero C, Jin DJ, Xiao J. 2019. Spatial organization of RNA polymerase and its relationship with transcription in *Escherichia coli*. Proc Natl Acad Sci U S A 116:20115– 20123. https://doi.org/10.1073/pnas.1903968116
- Holmes SF, Erie DA. 2003. Downstream DNA sequence effects on transcription elongation. Allosteric binding of nucleoside triphosphates facilitates translocation via a ratchet motion. J Biol Chem 278:35597– 35608. https://doi.org/10.1074/jbc.M304496200
- Stephanie F, Tambunan USF, Siahaan TJ. 2022. M. tuberculosis transcription machinery: a review on the mycobacterial RNA polymerase and drug discovery efforts. Life (Basel) 12:1774. https://doi.org/10.3390/ life12111774
- Hubin EA, Lilic M, Darst SA, Campbell EA. 2017. Structural insights into the mycobacteria transcription initiation complex from analysis of X-ray crystal structures. Nat Commun 8:16072. https://doi.org/10.1038/ ncomms16072

 Bao Y, Cao X, Landick R. 2024. RNA polymerase SI3 domain modulates global transcriptional pausing and pause-site fluctuations. Nucleic Acids Res 52:4556–4574. https://doi.org/10.1093/nar/gkae209

- Boyaci H, Saecker RM, Campbell EA. 2020. Transcription initiation in mycobacteria: a biophysical perspective. Transcription 11:53–65. https://doi.org/10.1080/21541264.2019.1707612
- Murakami KS, Masuda S, Campbell EA, Muzzin O, Darst SA. 2002. Structural basis of transcription initiation: an RNA polymerase holoenzyme-DNA complex. Science 296:1285–1290. https://doi.org/10. 1126/science.1069595
- Stallings CL, Stephanou NC, Chu L, Hochschild A, Nickels BE, Glickman MS. 2009. CarD is an essential regulator of rRNA transcription required for *Mycobacterium tuberculosis* persistence. Cell 138:146–159. https://doi. org/10.1016/j.cell.2009.04.041
- Czyz A, Mooney RA, Iaconi A, Landick R. 2014. Mycobacterial RNA polymerase requires a U-tract at intrinsic terminators and is aided by NusG at suboptimal terminators. MBio 5:e00931. https://doi.org/10. 1128/mBio.00931-14
- Gill SK, Garcia GA. 2011. Rifamycin inhibition of WT and Rif-resistant Mycobacterium tuberculosis and Escherichia coli RNA polymerases in vitro. Tuberculosis (Edinb) 91:361–369. https://doi.org/10.1016/j.tube.2011.05. 002
- Delbeau M, Omollo EO, Froom R, Koh S, Mooney RA, Lilic M, Brewer JJ, Rock J, Darst SA, Campbell EA, Landick R. 2023. Structural and functional basis of the universal transcription factor NusG pro-pausing activity in Mycobacterium tuberculosis. Mol Cell 83:1474–1488. https://doi.org/10. 1016/j.molcel.2023.04.007
- Boyaci H, Chen J, Lilic M, Palka M, Mooney RA, Landick R, Darst SA, Campbell EA. 2018. Fidaxomicin jams Mycobacterium tuberculosis RNA polymerase motions needed for initiation via RbpA contacts. Elife 7:e34823. https://doi.org/10.7554/eLife.34823
- Kouba T, Koval' T, Sudzinová P, Pospíšil J, Brezovská B, Hnilicová J, Šanderová H, Janoušková M, Šiková M, Halada P, Sýkora M, Barvík I, Nováček J, Trundová M, Dušková J, Skálová T, Chon Ur, Murakami KS, Dohnálek J, Krásný L. 2020. Mycobacterial HelD is a nucleic acidsclearing factor for RNA polymerase. Nat Commun 11:6419. https://doi. org/10.1038/s41467-020-20158-4
- Jacobs RQ, Bellis NF, Lucius AL, Schneider DA. 2023. Protocol for monitoring and analyzing single nucleotide incorporation by S. cerevisiae RNA polymerases. STAR Protoc 4:102191. https://doi.org/10. 1016/j.xpro.2023.102191
- Jacobs RQ, Ingram ZM, Lucius AL, Schneider DA. 2021. Defining the divergent enzymatic properties of RNA polymerases I and II. J Biol Chem 296:100051. https://doi.org/10.1074/jbc.RA120.015904
- Jacobs RQ, Carter ZI, Lucius AL, Schneider DA. 2022. Uncovering the mechanisms of transcription elongation by eukaryotic RNA polymerases I, II, and III. i Sci 25:105306. https://doi.org/10.1016/j.isci.2022.105306
- Carter ZI, Jacobs RQ, Schneider DA, Lucius AL. 2023. Transient-state kinetic analysis of the RNA polymerase II nucleotide incorporation mechanism. Biochemistry 62:95–108. https://doi.org/10.1021/acs. biochem.2c00608
- Appling FD, Lucius AL, Schneider DA. 2015. Transient-state kinetic analysis of the RNA polymerase I nucleotide incorporation mechanism. Biophys J 109:2382–2393. https://doi.org/10.1016/j.bpj.2015.10.037
- Fuller KB, Jacobs RQ, Schneider DA, Lucius AL. 2024. Reversible kinetics in multi-nucleotide addition catalyzed by S. cerevisiae RNA polymerase II reveal slow pyrophosphate release. J Mol Biol 436:168606. https://doi. org/10.1016/j.jmb.2024.168606
- Fuller KB, Jacobs RQ, Schneider DA, Lucius AL. 2023. The A12.2 subunit plays an integral role in pyrophosphate release of RNA polymerase I. J Mol Biol 435:168186. https://doi.org/.org/10.1016/j.jmb.2023.168186
- Cooper SL, Lucius AL, Schneider DA. 2024. Quantifying the impact of initial RNA primer length on nucleotide addition by RNA polymerase I. Biophys Chem 305:107151. https://doi.org/10.1016/j.bpc.2023.107151
- Ingram ZM, Scull NW, Schneider DS, Lucius AL. 2021. Multi-start evolutionary nonlinear opTimizeR (MENOTR): a hybrid parameter optimization toolbox. Biophys Chem 279:106682. https://doi.org/10. 1016/j.bpc.2021.106682
- Hao Z, Epshtein V, Kim KH, Proshkin S, Svetlov V, Kamarthapu V, Bharati
   B, Mironov A, Walz T, Nudler E. 2021. Pre-termination transcription

- complex: structure and function. Mol Cell 81:281–292 https://doi.org/10.1016/j.molcel.2020.11.013
- Chakravorty S, Helb D, Burday M, Connell N, Alland D. 2007. A detailed analysis of 16S ribosomal RNA gene segments for the diagnosis of pathogenic bacteria. J Microbiol Methods 69:330–339. https://doi.org/ 10.1016/j.mimet.2007.02.005
- Foster JE, Holmes SF, Erie DA. 2001. Allosteric binding of nucleoside triphosphates to RNA polymerase regulates transcription elongation. Cell 106:243–252. https://doi.org/10.1016/s0092-8674(01)00420-2
- Gelles J, Landick R. 1998. RNA polymerase as a molecular motor. Cell 93:13–16. https://doi.org/10.1016/s0092-8674(00)81140-x
- Nudler E, Avetissova E, Markovtsov V, Goldfarb A. 1996. Transcription processivity: protein-DNA interactions holding together the elongation complex. Science 273:211–217. https://doi.org/10.1126/science.273. 5272.211
- Shi J, Wen A, Zhao M, Jin S, You L, Shi Y, Dong S, Hua X, Zhang Y, Feng Y.
   Structural basis of Mfd-dependent transcription termination.
   Nucleic Acids Res 48:11762–11772. https://doi.org/10.1093/nar/gkaa904
- Xue Y, Hogan BP, Erie DA. 2000. Purification and initial characterization of RNA polymerase from thermus thermophilus strain HB8. Biochemistry 39:14356–14362. https://doi.org/10.1021/bi0012538
- Johnson GE, Lalanne JB, Peters ML, Li GW. 2020. Functionally uncoupled transcription-translation in *Bacillus subtilis*. Nature New Biol 585:124– 128. https://doi.org/10.1038/s41586-020-2638-5
- Jayasinghe OT, Mandell ZF, Yakhnin AV, Kashlev M, Babitzke P. 2022.
   Transcriptome-wide effects of NusA on RNA polymerase pausing in Bacillus subtilis. J Bacteriol 204:e0053421. https://doi.org/10.1128/jb. 00534-21
- Minakhin L, Nechaev S, Campbell EA, Severinov K. 2001. Recombinant thermus aquaticus RNA polymerase, a new tool for structure-based analysis of transcription. J Bacteriol 183:71–76. https://doi.org/10.1128/ JB.183.1.71-76.2001
- Lilic M, Chen J, Boyaci H, Braffman N, Hubin EA, Herrmann J, Müller R, Mooney R, Landick R, Darst SA, Campbell EA. 2020. The antibiotic sorangicin a inhibits promoter DNA unwinding in a *Mycobacterium* tuberculosis rifampicin-resistant RNA polymerase. Proc Natl Acad Sci U S A 117:30423–30432. https://doi.org/10.1073/pnas.2013706117
- Rue-Albrecht K, Magee DA, Killick KE, Nalpas NC, Gordon SV, MacHugh DE. 2014. Comparative functional genomics and the bovine macrophage response to strains of the mycobacterium genus. Front Immunol 5:536. https://doi.org/10.3389/fimmu.2014.00536
- Tomasselli AG, Marquetant R, Noda LH, Goody RS. 1984. The use of nucleotide phosphorothioate diastereomers to define the structure of metal-nucleotide bound to GTP-AMP and ATP-AMP phosphotransferases from beef-heart mitochondria. Eur J Biochem 142:287–289. https://doi. org/10.1111/j.1432-1033.1984.tb08283.x
- Abdullah Al Awadh A. 2022. Nucleotide and nucleoside-based drugs: past, present, and future. Saudi J Biol Sci 29:103481. https://doi.org/10. 1016/j.sjbs.2022.103481
- Serpi M, Ferrari V, Pertusati F. 2016. Nucleoside derived antibiotics to fight microbial drug resistance: new utilities for an established class of drugs? J Med Chem 59:10343–10382. https://doi.org/10.1021/acs. imedchem.6b00325
- Kay AW, Ness TE, Martinez L, Mandalakas AM. 2020. It ain't over till it's over: the triple threat of COVID-19, TB, and HIV. Am J Trop Med Hyg 103:1348–1349. https://doi.org/10.4269/ajtmh.20-1089
- Derissen EJB, Beijnen JH. 2020. Intracellular pharmacokinetics of pyrimidine analogues used in oncology and the correlation with drug action. Clin Pharmacokinet 59:1521–1550. https://doi.org/10.1007/ s40262-020-00934-7
- Seley-Radtke KL, Yates MK. 2018. The evolution of nucleoside analogue antivirals: a review for chemists and non-chemists. Antiviral Res 154:66– 86. https://doi.org/10.1016/j.antiviral.2018.04.004
- World Health Organization. 2023. Global tuberculosis report 2023. World Health Organization, Geneva, Switzerland. Available from: https://www. who.int/news-room/fact-sheets/detail/tuberculosis
- Jin DJ, Turnbough CL. 1994. An Escherichia coli RNA polymerase defective in transcription due to its overproduction of abortive initiation products. J Mol Biol 236:72–80. https://doi.org/10.1006/jmbi.1994.1119